Chemistry Journals

Analytical, Inorganic, Organic, Physical, Materials Science

2D hexagonal boron nitride for solar energy conversions

Amall Ahmed Ramanathan [Corresp. 1]

1 The University of Jordan, Amman, Jordan

Corresponding Author: Amall Ahmed Ramanathan
Email address: amallahmad@gmail.com

The optoelectronic properties of free standing monolayer (ML) hexagonal boron nitride (h-BN) is investigated for potential solar energy conversion applications using the Density Functional Theory (DFT) full potential linearized augmented plane wave (FP-LAPW) method. In addition, the bulk optical properties have also been calculated for the sake of comparison. The dielectric functions, optical conductivities and the optical constants are evaluated using the relaxed structures from electronic total energy pseudopotential calculations. The results reinforce previous research on h-BN DUV optoelectronics and demonstrate the suitability of its use as a component in deep ultraviolet (DUV) and energy conversion devices.

2D hexagonal boron nitride for solar energy conversions

6 Amall Ahmed Ramanathan

8 Department of Physics, The University of Jordan, Amman, Jordan

10 Corresponding Author:
11 Amall Ramanathan
12 University Street, Amman, 11941, Jordan
13 Email address: corresponding author_ amallahmad@gmail.com

Abstract

16 The optoelectronic properties of a free standing monolayer (ML) of hexagonal boron nitride (h-
17 BN) is investigated for potential solar energy conversion applications using the Density
18 Functional Theory (DFT) full potential linearized augmented plane wave (FP-LAPW) method. In
19 addition, the bulk optical properties have also been calculated for the sake of comparison. The
20 dielectric functions, optical conductivities and the optical constants are evaluated using the
21 relaxed structures from electronic total energy pseudopotential calculations. The results reinforce
22 previous research on h-BN DUV optoelectronics and demonstrate the suitability of its use as a
23 component in deep ultraviolet (DUV) and energy conversion devices.

24

25 Key words: DFT_PAW; DUV; dynamic electrical conductivity; dielectric function, optical
26 constants

27

Introduction

29 The last two decades have seen tremendous research on two-dimensional (2D) materials similar
30 to graphene; which was the first 2D material discovered with a honeycomb structure consisting
31 of single layers of carbon atoms and endowed with remarkable electronic, mechanical and
32 optical properties [1-4]. Especially, layered transition metal dichalcogenides (TMDs) are widely
33 investigated due to the rich diversity of properties which can be attributed to the finite and
34 tuneable bandgap in these materials and have seen a multitude of applications [5-8].
35 In comparison to TMDs a less researched graphene analog is h-BN that is now gaining
36 popularity as the key building block in van der Waal hetrostructures [9]. Each B^{3+} atom is
37 bonded in a trigonal planar geometry to three equivalent N^{3-} atoms and vice versa as shown in
38 Figure 1. Similar to graphene, 2D h-BN has a honeycomb structure and consists of alternating B
39 and N atoms that are sp^2 covalently bonded, but, it has an insulating character. Moreover, due to

40 the difference in electronegativity of the B and N atoms, the bond between B and N shows an
41 ionic character and it is not purely covalent as in graphene. Being the structural analog of
42 graphene h-BN is expected to possess and it does show excellent mechanical properties and high
43 chemical and thermal stabilities [10-12]. The small mismatch in lattice parameter of h-BN with
44 graphene and the absence of dangling bonds and charge traps makes it an ideal substrate for
45 graphene based devices [13, 14]. The indirect to direct bandgap crossover in MLs of TMDs with
46 its efficient light matter coupling is also observed in h-BN [15, 16] and makes it a promising
47 material for optoelectronics and deep ultraviolet (DUV) applications [17-19].
48 It is now the age of nano electronics and with the increasingly small size of components there is
49 a need to extend optical systems to shorter wavelengths than visible light to improve the image
50 resolution. This has motivated the interest in the short-wave UV region, especially DUV optics.
51 The focus of the present study is to investigate the dynamic electrical conductivity and optical
52 constants in order to better understand and substantiate previous research on h-BN DUV
53 optoelectronics and its possible use as a component in solar energy conversion devices.
54

Method

56 The calculations are carried out in two steps. First, DFT calculations using the ABINIT software
57 program [20] with the generalized gradient approximation (GGA) projector augmented wave
58 (PAW) pseudopotentials [21] are performed for structural optimization as in previous works [22,
59 23]. Convergence criteria of less than 1×10^{-6} Ha for the Self Consistent Field (SCF) iterations
60 and force threshold of less than 1 mRy/a.u. for structural optimizations are used with the
61 optimized k-point grids of $10 \times 10 \times 10$ and $10 \times 10 \times 5$ for h-BN bulk and ML h-BN respectively
62 and a cutoff energy of 20Ha to obtain the lattice constants and relaxed structures.
63 Next, the relaxed geometries that have been obtained are used to perform FP-LAPW calculations
64 with the WIEN2k [24] code employing GGA_PBE to obtain the ground state energies and band
65 structures. The wave functions in interstitial region were expanded in plane waves with a cutoff
66 of Rmt*Kmax set to 7 for energy eigenvalues convergence; Kmax gives the magnitude of the
67 largest K vector in the plane-wave expansion and the muffin-tin radii (Rmt) are set to 1.37 and
68 1.36 a.u for both the atoms in the bulk and ML h-BN respectively. K-point grids of $10 \times 10 \times 10$
69 and $15 \times 15 \times 2$ are used for the electronic calculations of the bulk and ML respectively. More
70 stringent calculations using denser grids of $19 \times 19 \times 6$ and $50 \times 50 \times 2$ are used for the bulk and ML
71 h-BN respectively to evaluate the optical properties, namely the frequency dependent
72 conductivities, real and imaginary parts of dielectric tensor, index of refraction, reflectivity and
73 the absorption and extinction coefficients.
74

Results

Structural and electronic

77 The Simulation of the 2D BN in the hexagonal structure is done by using the supercell technique.
78 The optimized value of the bulk lattice constant is used to set up the super cell that contains a
79 single atomic layer of h-BN separated by sufficient amount of vacuum in the z direction to offset

80   any interactions between layers. The free standing h-BN ML is relaxed to obtain the ground
81   state. The bulk and ML structures of h-BN are shown in Fig S1. The lattice constant values and
82   band gaps for the optimized bulk and ML are listed in Table 1 and are consistent with those of
83   other experimental and GGA-PBE calculations [16, 25-28]. The band structures of the bulk and
84   ML h-BN are presented in Fig S2. We see an indirect K−M (bulk) to direct K−K band (ML)
85   transition, consistent with recent results showing a direct wide bandgap value of 4.65 eV in the
86   ML. This is also in accordance with other 2D materials like MoS_2 which show and indirect to
87   direct band cross over when going from the bulk to the ML [8, 29]. In the past there was a
88   controversy about the nature of the bandgap of h-BN bulk and ML, but, with the recent
89   experimental evidence using optical spectroscopy of Cassabois et al [15] and the work of Elias et
90   al [16] who used a combination of deep-ultraviolet photoluminescence and reflectance
91   spectroscopy with atomic force microscopy, it is now confirmed that there is an indirect to direct
92   bandgap crossover in h-BN bulk to the ML. The bandgap is much smaller than experiment in this
93   work due to the well known problem of underestimation of GGA-DFT works.
94
95   **Dynamical optical conductivities and constants**
96   The term "optical conductivity" means the electrical conductivity in the presence of an
97   alternating electric field or dynamic electrical conductivity. The term "optical" here implies the
98   entire frequency range, and is not restricted to just the visible region. The imaginary part of the
99   dielectric constant is related to the real part of the AC conductivity and, therefore, to the optical
100   reflectivity and transmittance [30]. The real part of the dynamic electrical conductivity is
101   connected with the energy absorbed by the electrons. The imaginary part of dielectric function,
102   $\varepsilon_2(\omega)$, which represents absorption behavior, can be calculated from the electronic band structure.
103   The real part of dielectric function, $\varepsilon_1(\omega)$, can be calculated according to Kramers-Kroing
104   relation [31] which represents the electronic polarization under incident light. The optical
105   conductivity and absorption behaviour of ML h-BN with respect to the photon energies are
106   shown in Figure 2. We see from the figure the maximum conductivity and absorption peaks are
107   at ~ 6, 11 and 13.5eV that is in the mid-UV and DUV regions considering the in-plane xx and
108   perpendicular zz directions. There is also a small shoulder at around 4.5eV. We also note that
109   both the xx and zz directions have almost similar magnitudes for the conductivity and absorption
110   coefficients $\alpha(\omega)$. The absorption coefficient peak value is in good agreement with the
111   experimental work of Li et al [32].
112   A comparison with the supplementary information Figure S3 and S6 shows that the ML h-BN
113   retains the bulk characteristics for the conductivities and absorption coefficients $\alpha(\omega)$, however,
114   their magnitudes in the bulk are almost three times and two times more than the ML h-BN values
115   respectively.
116   Figure 3 depicts the real and imaginary parts of the dielectric constant for the ML h-BN. The
117   static values of the real dielectric constant are around 1.6 and 1.2 in the xx and zz directions
118   respectively. Figs. 2(a) and (b) curves show the anisotropic behaviour in the two directions as in
119   the previous conduction and absorption spectra Fig. 2.

120 However, for bulk h-BN, a look at Figure S4 shows that the static real dielectric constants are
121 almost double in value around 3.6 and 2.3 in the in-plane and perpendicular directions
122 respectively. A comparison of the magnitudes of the first sharp peaks of the imaginary dielectric
123 constants Figs. 3(b) and S4(b) indicate the higher absorption capabilities of bulk as compared to
124 that of ML h-BN.
125 From the values of $\varepsilon_1(\omega)$ and $\varepsilon_2(\omega)$ we can obtain the refractive index $n(\omega)$, reflectivity $R(\omega)$ and
126 the extinction and absorption coefficients $k(\omega)$ and $\alpha(\omega)$ respectively from the relevant equations
127 as detailed in the work [33]. The refractive index and extinction coefficients are shown in Fig. 4.
128 Once again we notice the anisotropy in the xx and zz directions. The static refractive index
129 values obtained are 1.3 and 1.1 in the in-plane and out of plane directions respectively and ML h-
130 BN is transparent in the IR and visible region for xx direction and also in mid-DUV for the zz
131 direction as evinced from the flatness of the curves. A direct comparison of the refractive indices
132 of the bulk and ML is depicted in S5 and we see that the bulk values are consistently higher at
133 1.9 and 1.5 in the xx and zz directions respectively and reflect the higher electron density in the
134 bulk. For the sake of better readability the static values of the refractive indices, the reflectivity
135 and absorption coefficients for the bulk and ML h-BN in both the in-plane xx and out of plane zz
136 directions have been gathered in Table 2. The table also includes the energies at the zero values
137 of $\varepsilon_1(\omega)$.
138 The reflectivity plots for the ML and bulk h-BN are represented in Figure 5. The static values of
139 reflectivity are very low both for ML and bulk h-BN and continues to be low over a wide range
140 of photon energies 0-9eV for the perpendicular component which peaks in DUV region.
141 Whereas, for the in-plane direction the reflectivity values are low in the visible and the first peak
142 is around 6eV.
143

Discussion

145 The electronic structure calculations in this work confirms the previous literature results [15, 16,
146 27, 28] of the bandgap crossover of indirect to direct in h-BN bulk to ML. However, although
147 the band gap values are in fair agreement with other theoretical works it is underestimated in
148 comparison with experimental findings of 6.1eV in ML h-BN [16] due to the shortcomings of the
149 GGA exchange correlation potential. A more accurate calculation using the Modified Becke-
150 Johnson (mBJ) approximation [34, 35] is expected to give a better estimate for the bandgap and
151 is part of future work.
152 The optical properties are qualitatively consistent with other theoretical and experimental works
153 [16, 32, 36-38] and reinstate the importance of h-BN in DUV optoelectronics. Essentially the h-
154 BN ML mimics the behaviour of the bulk and the shape and peak positions for the optical
155 conductivity and constants are similar but the magnitude is much lower owing to the higher
156 values of the dielectric constants in the bulk. Since, the attractive wide band and optical
157 properties in DUV is maintained in the ML h-BN, with the added advantage of a direct bandgap,
158 ML h-BN is a promising candidate for nano-optoelectronics in the DUV region. Numerous
159 applications as DUV photo detectors/emitters, possible integration with graphene optoelectronics

160 due its flatness and similarity in structure and close lattice constant values, and in addition, its
161 promise for realizing chip-scale DUV light sources are all waiting to be realized. Moreover, it
162 can be argued that the optical properties of h-BN in the ultraviolet are very useful for the study of
163 peptides and other biomolecules [16, 39, 40].
164

Conclusions

166 In conclusion, the study of the optoelectronic properties of ML h-BN using first principles FP-
167 LAPW method with the GGA approximation shows an indirect K−M to direct K−K band
168 transition when going from the bulk to the ML with a wide bandgap value of 4.65 eV, consistent
169 with recent results. The excellent values of conductivity and absorption in the mid UV and DUV
170 uphold the great promise of this material for use in DUV optics and energy conversions. A more
171 accurate calculation using mBJ exchange correlation to reconfirm these very interesting optical
172 properties is highly desirable and is the future direction.
173

Acknowledgements

176 This work has been carried out at the   theoretical physics laboratory, department of
177 Physics at the University of Jordan.

178

References

180 1. Max C. Lemme, "Current Status of Graphene Transistors", Solid State Phenomena, 156-
181   158, Pages 499-509, 2010.
182 2. Garnica B, S. A., Knaust, M., & Fatikow, S. (2019). Automatic Micro-Robotic
183   Identification and Electrical Characterization of Graphene. *Micromachines*, *10*(12), 870.
184 3. Aqra M.W. and Ramanathan A.A. Graphene and related 2D materials for desalination: A
185   review of recent patents. *Jordan J. Phys*. 2020, *13 (3)* 233-242
186 4. Szunerits, S., and Boukherroub, R. Graphene-based biosensors. *Interface Focus* 2018
187   8:20160132. doi: 10.1098/rsfs.2016.0132
188 5. Ramanathan AA and Khalifeh JM (2018). Enhanced thermoelectric properties of
189   suspended mono and bilayer of MoS_2 from first principles. IEEE Transactions on
190   nanotechnology, 17(5), 974
191 6. Chen, Y.; Tan, C.; Zhang, H.; Wang, L. Two-Dimensional Graphene Analogues for
192   Biomedical Applications. *Chem. Soc. Rev.* 2015.
193 7. D. Vikraman, K. Akbar, S. Hussain, G. Yoo, J-Y. Jang, S-H. Chun, J. Jung, H.J. Park:
194   Direct synthesis of thickness-tunable MoS_2 quantum dot thin layers: Optical, structural
195   and electrical properties and their application to hydrogen evolution. *Nano Energy*, **35**,
196   101 (2017).
197 8. Ramanathan AA and Khalifeh JM (2021). Thermoelectrics of $MoS_{2(1-x)}N_{2x}$ compounds.
198   DOI: 10.23880/psbj-16000167
199 9. Geim, A. K. & Grigorieva, I. V. Van der Waals heterostructures. Nature 499,419–425
200   (2013).

201   10. Zhi, C. Y.; Bando, Y. ; Tang, C. C.; Kuwahara, H.; Golberg, D. Large-scale fabrication
202   of boron nitride nanosheets and their utilization in polymeric composites with improved
203   thermal and mechanical properties. Adv. Mater. 2009, 21, 2889.
204   11. Grosjean, B., Pean, C., Siria, A., Bocquet, L., Vuilleumier, R., & Bocquet, M. L. (2016).
205   Chemisorption of Hydroxide on 2D Materials from DFT Calculations: Graphene versus
206   Hexagonal Boron Nitride. *The journal of physical chemistry letters*, *7*(22), 4695–4700.
207   12. Ramanathan AA., Aqra MW and Al-Rawajfeh AE Recent advances in 2D- nanopores for
208   desalination. ECLE 2018, 16(4) 1217-1231.
209   13. Wang, M., Jang, S. K., Jang, W. J., Kim, M., Park, S. Y., Kim, S. W., Kahng, S. J., Choi,
210   J. Y., Ruoff, R. S., Song, Y. J., & Lee, S. (2013). A platform for large-scale graphene
211   electronics--CVD growth of single-layer graphene on CVD-grown hexagonal boron
212   nitride. Advanced materials, *25*(19), 2746–2752.
213   14. Khan, A., Islam, S. M., Ahmed, S., Kumar, R. R., Habib, M. R., Huang, K., Hu, M., Yu,
214   X., & Yang, D. (2018). Direct CVD Growth of Graphene on Technologically Important
215   Dielectric and Semiconducting Substrates. Advanced science, *5*(11), 1800050.
216   15. Cassabois, G., Valvin, P. & Gil, B. Hexagonal boron nitride is an indirect bandgap
217   semiconductor. Nat. Photon. 10, 262–266 (2016)
218   16. Elias, C., Valvin, P., Pelini, T. *et al.* Direct band-gap crossover in epitaxial monolayer
219   boron nitride. Nat Commun 10, 2639 (2019).
220   17. Watanabe, K., Taniguchi, T. & Kanda, H. Direct-bandgap properties and evidence for
221   ultraviolet lasing of hexagonal boron nitride single crystal. Nat. Mater. 3, 404–409
222   (2004).
223   18. Liu, H., Meng, J., Zhang, X., Chen, Y., Yin, Z., Wang, D., Wang, Y., You, J., Gao, M., &
224   Jin, P. (2018). High-performance deep ultraviolet photodetectors based on few-layer
225   hexagonal boron nitride. *Nanoscale*, *10*(12), 5559–5565.
226   19. Yin, J., Li, J., Hang, Y., Yu, J., Tai, G., Li, X., Zhang, Z. and Guo, W. (2016), Boron
227   Nitride Nanostructures: Fabrication, Functionalization and Applications. Small, 12: 2942-
228   2968.
229   20. X. Gonze, F. Jollet, F. A. Araujoa, D. Adams, B. Amadon, T. Applencourt et al (2016).
230   Recent developments in the ABINIT software package. Computer Physics
231   Communications 205, 106
232   21. J. P. Perdew, K. Burke, and M. Ernzerhof, Generalized Gradient Approximation Made
233   Simple, Phys. Rev. Lett. (1996) 77, 3865; Torrent, F. Jollet, F. Bottin, G. Zerah, and X.
234   Gonze Implementation of the Projector Augmented-Wave Method in the ABINIT code.
235   M Comput. Mat. Science 42, 337, (2008).
236   22. A. A. Ramanathan. A DFT calculation of Nb and Ta (001) Surface Properties, JMP_
237   Special issue-DFT 2013, *4*, 432-437.
238   23. A.A. Ramanathan and J.M Khalifeh (2017). Substrate matters: Magnetic tuning of the Fe
239   monolayer. JMMM 426, 450-453.

240 24. P. Blaha, K.Schwarz, F. Tran, R. Laskowski, G.K.H. Madsen and L.D. Marks, J. Chem.
241   Phys. (2020) 152, 074101
242 25. R. W. Lynch, H. G. Deickamer, Effect of High Pressure on the lattice Paramers of
243   Diamond, Graphite, and Hexagonal Boron Nitride. J. Chem. Phys. 44(1), 181–184
244   (1966).
245 26. Bin Xu, Meizhe Lv, Xiaohong Fan, Wen Zhang, Yong Xu & Tongguang Zhai (2015)
246   Lattice Parameters of Hexagonal and Cubic Boron Nitrides at High Temperature and
247   High Pressure. Integrated Ferroelectrics, 162:1, 85-93
248 27. Vuong, T. Q. P. et al. (2017) Phonon symmetries in hexagonal boron nitride probed by
249   incoherent light emission. 2D Mater. 4, 11004
250 28. Schuster, R., Habenicht, C., Ahmad, M., Knupfer, M. & Büchner (2018) B. Direct
251   observation of the lowest indirect exciton state in the bulk of hexagonal boron
252   nitride. Phys. Rev. B 97, 041201
253 29. Mak, K. F.; Lee, C.; Hone, J.; Shan, J.; Heinz, T. F. Atomically thin MoS2: A new direct-
254   gap semiconductor. Phys. Rev. Lett. 2010, 105, 136805.
255 30. Ashcroft, N.W. and Mermin, N.D. (1976) Solid State Physics, Saunders College
256   Publishing.
257 31. Kramers H A 1927 Atti del Congresso Internazionale dei Fisici vol 2 (Bologna:
258   Zanichelli) p 545; Kronig R de L 1926 J. Opt. Soc. Am. 12 547
259 32. Li J, Majety S, Dahal R, Zhao WP, Lin JY, Jiang HX. Dielectric strength, optical
260   absorption, and deep ultraviolet detectors of hexagonal boron nitride epilayers. Appl Phys
261   Lett 2012;101:67–92.
262 33. Ramanathan A.A.; Khalifeh J.M. Electronic, magnetic and optical properties of XScO3
263   (X=Mo, W) perovskites *PeerJ Materials Science* 3:e15 https://doi.org/10.7717/peerj-
264   matsci.15
265 34. F. Tran, P. Blaha, Accurate band gaps of semiconductors and insulators with a semilocal
266   exchange-correlation potential, Phys. Rev. Lett. 102 (2009) 226401.
267 35. Ramanathan, A.A. First Principles Investigation of the Optoelectronic Properties of
268   Molybdenum Dinitride for Optical Sensing Applications. *Chem. Proc.* 2021, 5, 27.
269 36. R. Gao, L. Yin, C. Wang, Y. Qi, N. Lun, L. Zhang, Y. X. Liu, L. Kang and X. Wang, J.
270   Phys. Chem. C, 2009, 113, 15160– 15165.
271 37. Wang J, Cao S, Sun P, Ding Y, Li Y, Ma F. Optical advantages of graphene on the boron
272   nitride in visible and SW-NIR regions. RSC Adv 2016;6:111345–9.
273 38. Wang, J., Ma, F., & Sun, M. (2017). Graphene, hexagonal boron nitride, and their
274   heterostructures: properties and applications. *RSC Advances, 7*, 16801-16822.
275 39. Ferreira F, Chaves A J, Peres N M R and Ribeiro R M 2019 Excitons in hexagonal boron
276   nitride single-layer: a new platform for polaritonics in the ultraviolet J. Opt. Soc. Am.
277   36 674

278   40. Henriques JCG, Ventura GB, Fernandes CDM and Peres NMR. Optical absorption of
279   single-layer hexagonal boron nitride in the ultraviolet. J. Phys.: Condens. Matter 32
280   (2020) 025304
281

Structural and electronic

Table 1 Structural and electronic properties of the relaxed h-BN

1   **Table 1** Structural and electronic properties of the relaxed h-BN bulk and ML

Compound	Space Group	Lattice constant (Å)		Bandgap (eV)		Inter layer spacing	Other works		
		a	c				a	c	bandgap
h-BN bulk	P63/mmc #194	2.517	6.706	4.23	K−M indirect	3.353	2.505[a] 2.511[b]	6.661[a] 6.688[b]	5.955[c]
h-BN ML	P-6 m 2 #187	2.515	15.063	4.65	K−K direct	-			6.1[d]

2   [a]Ref. 25 [b]Ref. 26   [c]Ref. 16, 27, 28 [d]Ref. 16

 Chemistry Journals
Analytical, Inorganic, Organic, Physical, Materials Science

Static values of optical properties

Table 2 The zero y-values of $\varepsilon_1(\omega)$ and the static optical constants (at ω=zero): dielectric constant $\varepsilon_1(0)$, refractive index n(0), reflectivity R(0) and absorption coefficient I(0) for the bulk and ML h-BN

1   **Table 2** The zero y-values of $\varepsilon_1(\omega)$ and the static optical constants (at ω=zero): dielectric constant $\varepsilon_1(0)$, refractive
2   index n(0), reflectivity R(0) and absorption coefficient I(0) for the bulk and ML h-BN

Compound	Zeros of $\varepsilon_1(\omega)$ [eV]		$\varepsilon_1(0)$		n(0)		R(0)		I(0)	
	XX	ZZ	XX	ZZ	XX	ZZ	XX	ZZ	XX	ZZ
hBN bulk	5.84; 9.13	11.22; 12.20	3.64	2.32	1.91	1.52	0.097	0.043	0.0055	0.0024
hBN ML	13.51	13.56	1.66	1.22	1.29	1.10	0.016	0.002	0.0021	0.0004

Chemistry Journals
Analytical, Inorganic, Organic, Physical, Materials Science

Figure 1

h-BN molecule

Figure 1 Illustration of an h-BN molecule
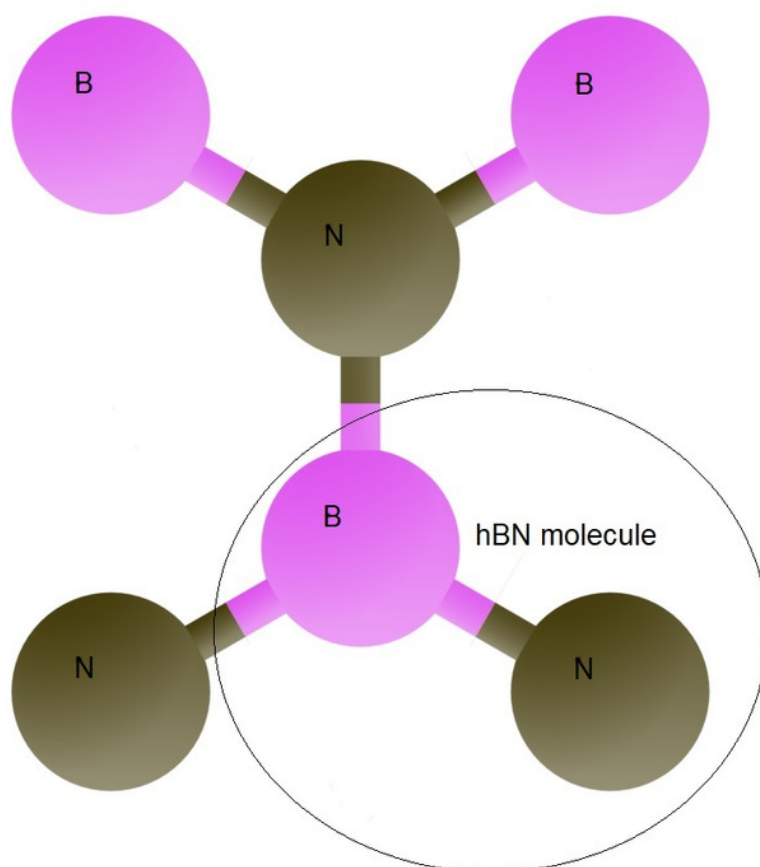
Figure 2

The Optical conductivity

Figure 2 (a). The optical conductivities for ML h-BN in the xx in-plane and zz out of plane directions.
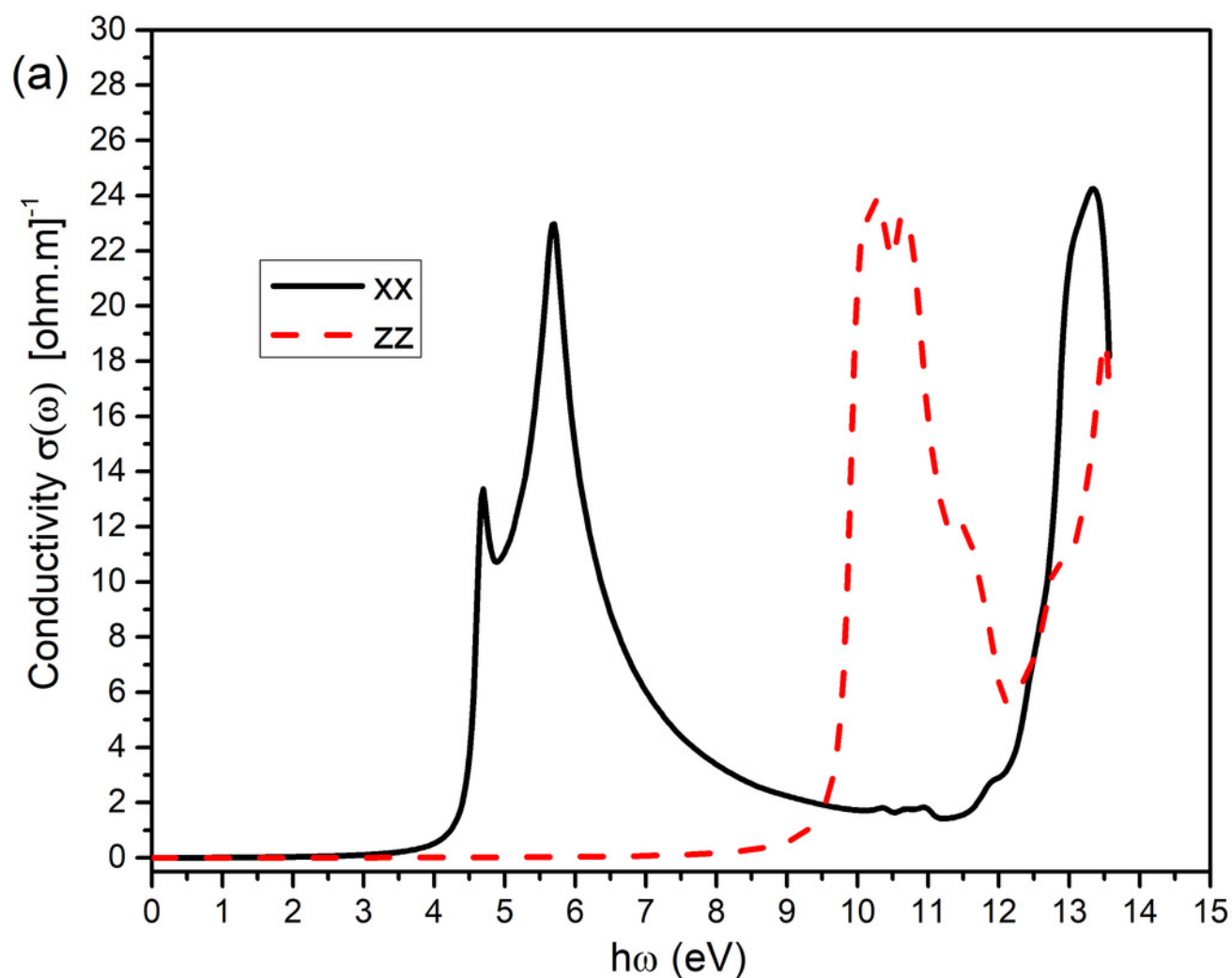
Figure 3

The absorption coefficient

Figure 2 (b). The absorption coefficients for ML h-BN in the xx in-plane and zz out of plane directions.
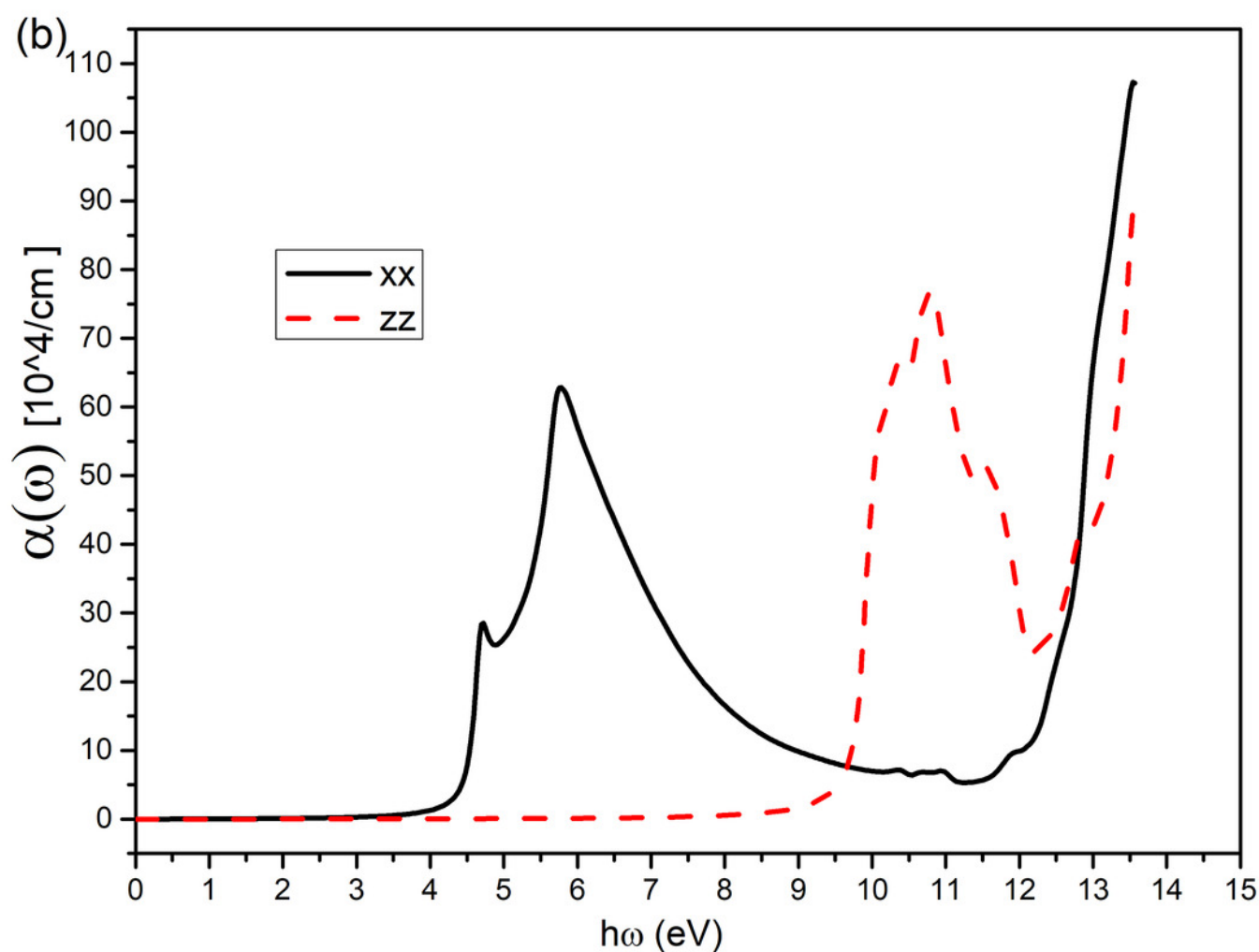
Figure 4

The dielectric function

Figure 3(a). The real parts of the dielectric function in the xx and zz directions for ML h-BN
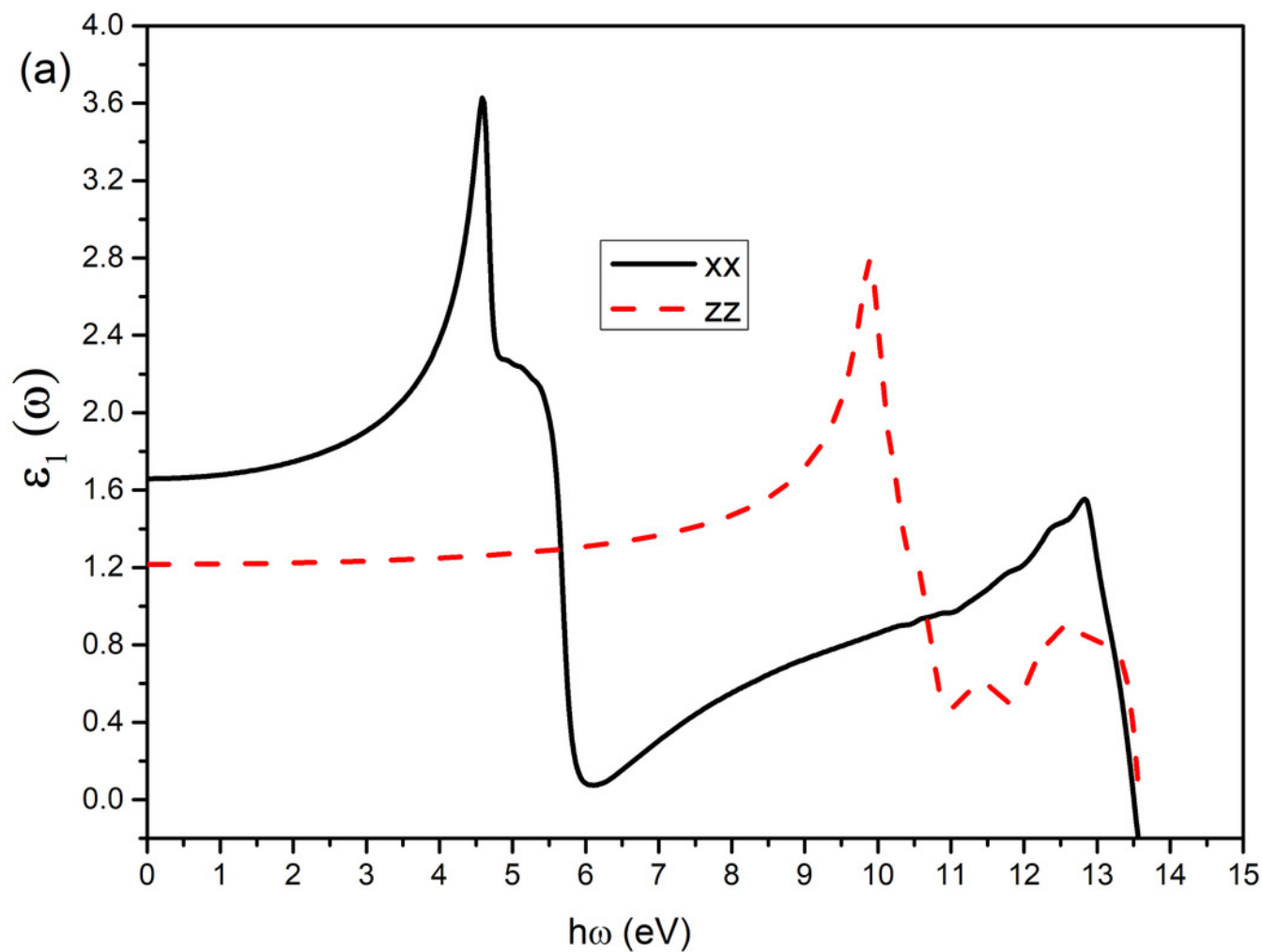
Figure 5

The dielectric function

Figure 3(b). The imaginary parts of the dielectric function in the xx and zz directions for ML h-BN
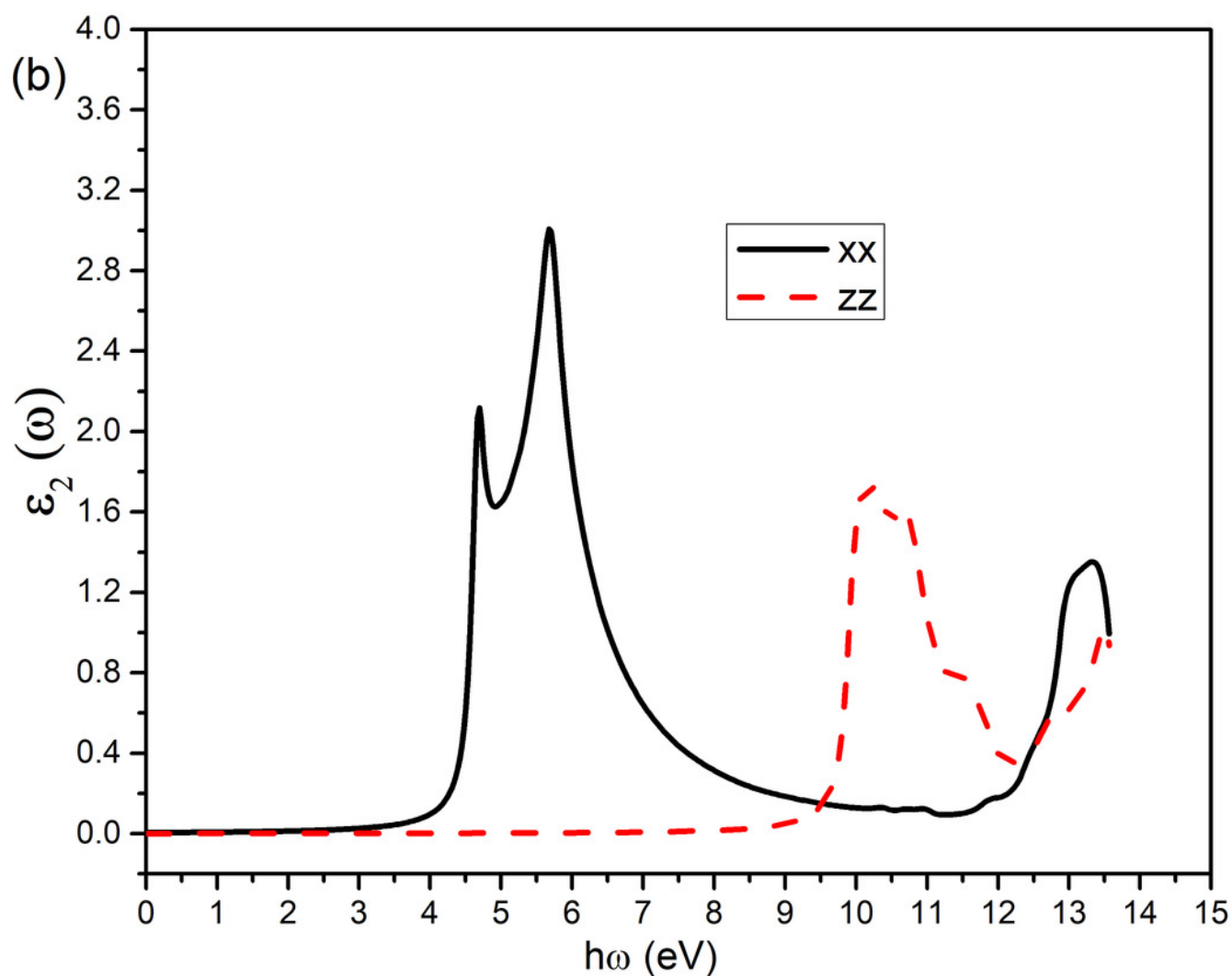
Figure 6

The refractive index

Figure 4(a). The refractive indices in the xx and zz directions for ML h-BN
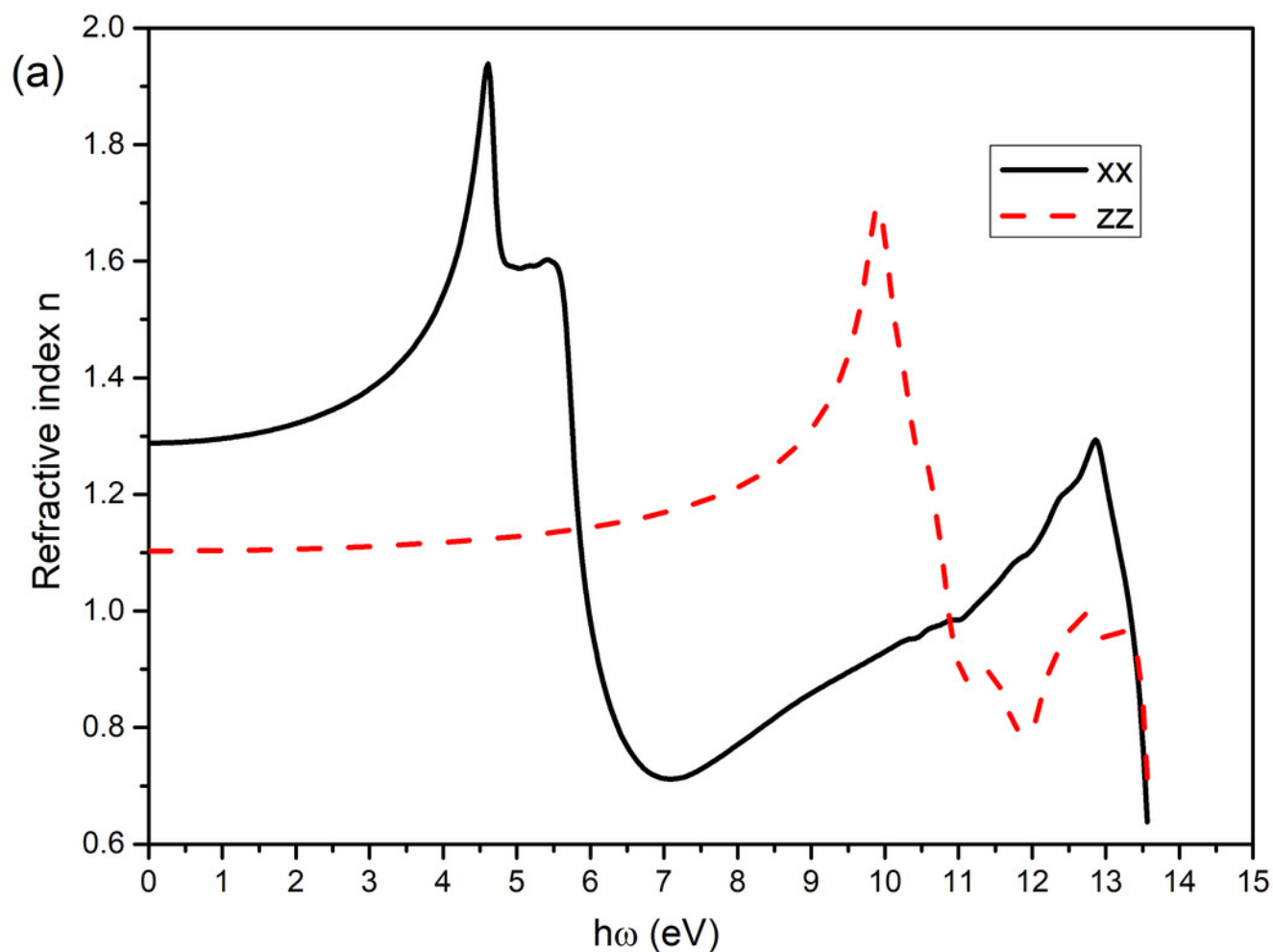
Figure 7

The extinction coefficient

Figure 4(b). The extinction coefficients in the xx and zz directions for ML h-BN
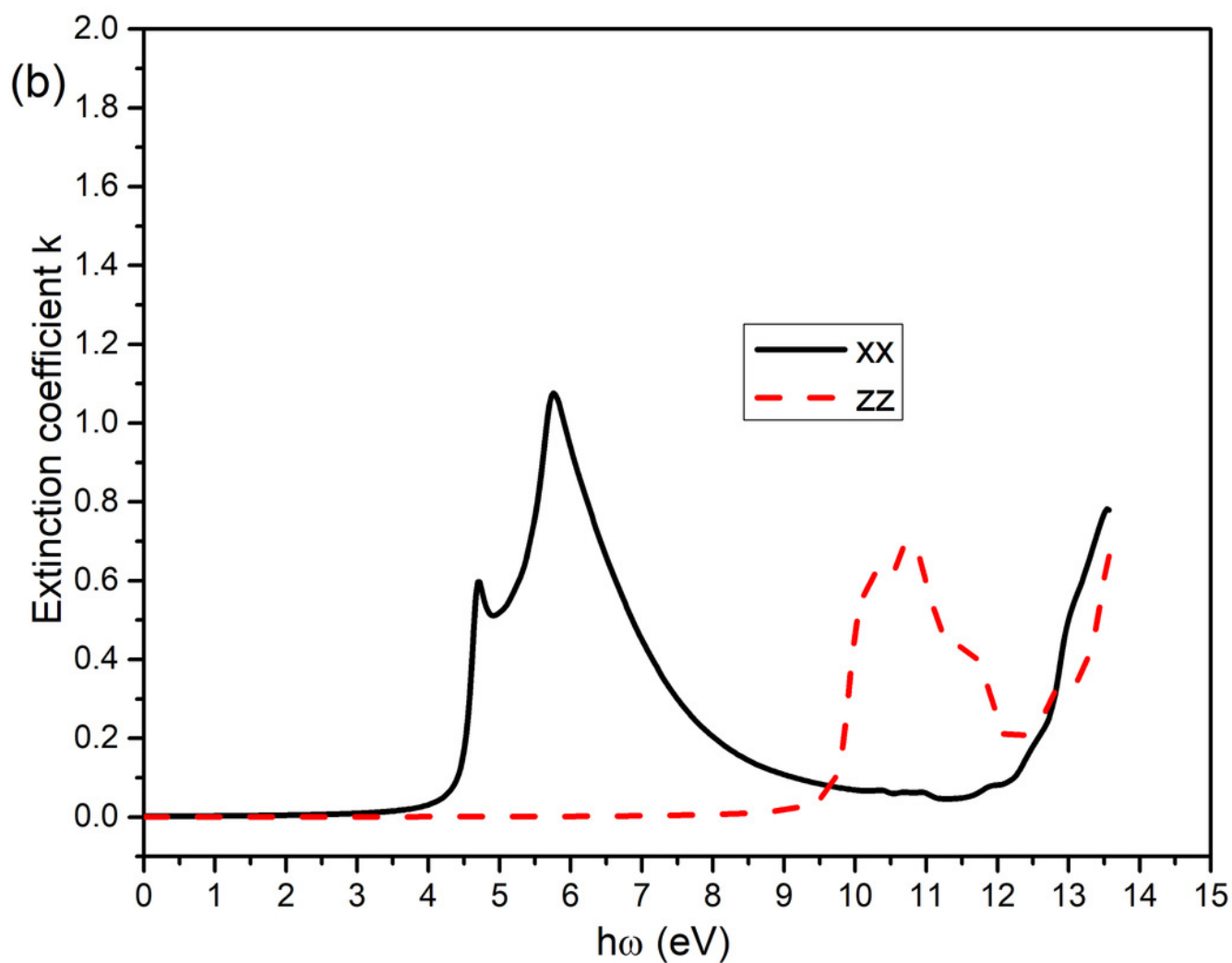
Figure 8

The reflectivity of ML h-BN

Figure 5(a). The reflectivity plots for ML h-BN in the xx and zz directions
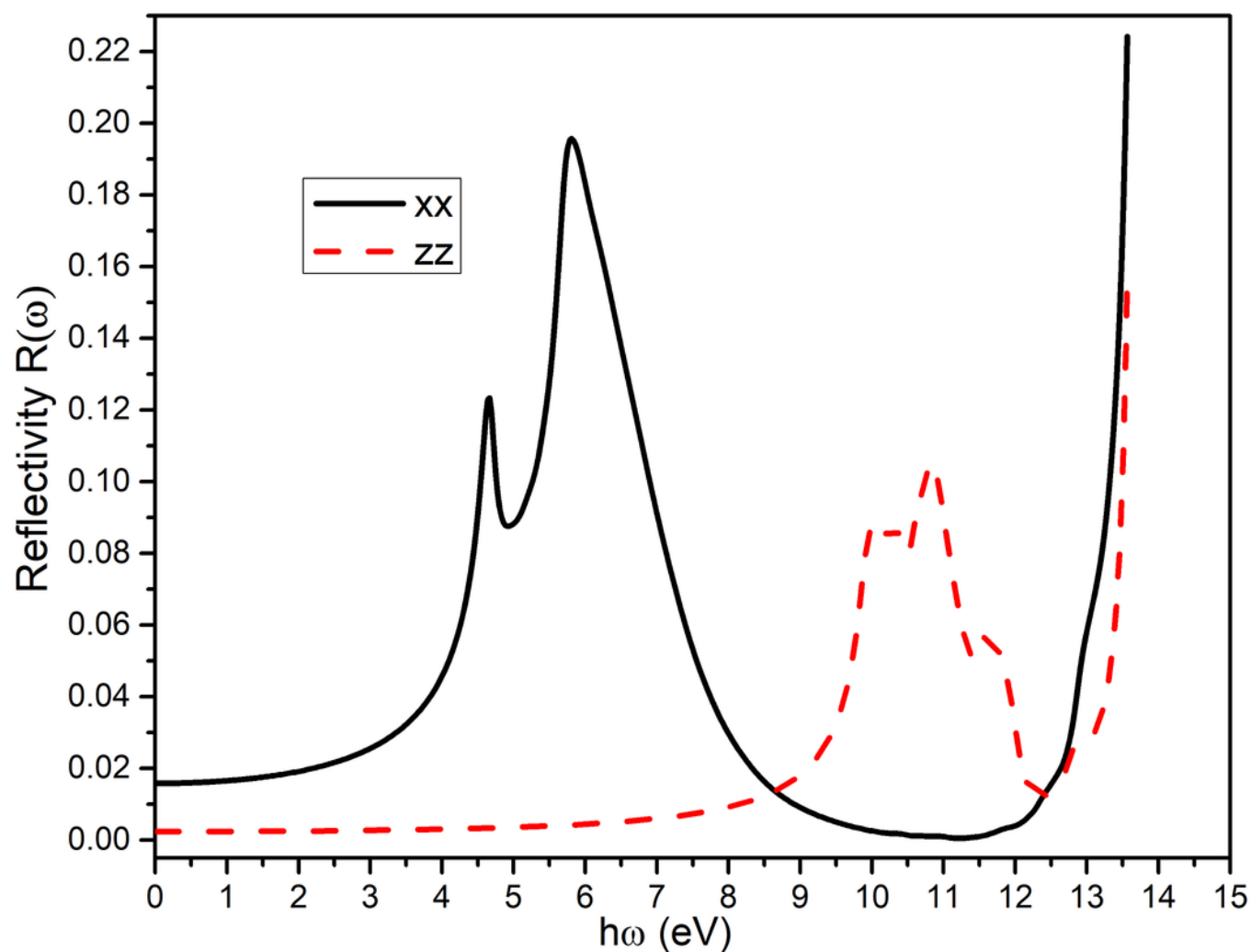
Figure 9

The bulk h-BN reflectivity

Figure 5(b). The reflectivity plots for bulk h-BN in the xx and zz directions